Electron-impact excitation of diatomic hydride cations II: OH+ and SH+

James R. Hamilton, Alexandre Faure, Jonathan Tennyson

Monthly Notices
of the
ROYAL ASTRONOMICAL SOCIETY

MNRAS **476,** 2931–2937 (2018)
Advance Access publication 2018 February 20

doi:10.1093/mnras/sty437

Electron-impact excitation of diatomic hydride cations II: OH^+ and SH^+

James R. Hamilton,[1] Alexandre Faure[2]★ and Jonathan Tennyson[1]★

[1]*Department of Physics and Astronomy, University College, London, Gower St., London WC1E 6BT, UK*
[2]*University Grenoble Alpes, CNRS, IPAG, F-38000 Grenoble, France*

Accepted 2018 February 8. Received 2018 February 8; in original form 2017 December 24

ABSTRACT

R-matrix calculations combined with the adiabatic-nuclei-rotation and Coulomb-Born approximations are used to compute electron-impact rotational rate coefficients for two open-shell diatomic cations of astrophysical interest: the hydroxyl and sulphanyl ions, OH^+ and SH^+. Hyperfine resolved rate coefficients are deduced using the infinite-order-sudden approximation. The propensity rule $\Delta F = \Delta j = \Delta N = \pm 1$ is observed, as is expected for cations with a large dipole moment. A model for OH^+ excitation in the Orion Bar photon-dominated region is presented which nicely reproduces *Herschel* observations for an electron fraction $x_e = 10^{-4}$ and an OH^+ column density of 3×10^{13} cm^{-2}. Electron-impact electronic excitation cross-sections and rate coefficients for the ions are also presented.

Key words: line: formation – molecular data; molecular processes – ISM: molecules.

1 INTRODUCTION

Cross-sections for electron collisions with molecular ions can be very large (>1000 Å^2). If the ion in question contains a permanent dipole moment, the electron-impact rotational excitation rate coefficients far exceed those of H and H_2 meaning that in comparatively electron-rich regions, electron collisions can become the dominant excitation process. Rotational rate coefficients have already been used to quantify interstellar electron densities (Jimenez-Serra et al. 2006; Harrison, Faure & Tennyson 2013; Hamilton, Faure & Tennyson 2016), but the rate coefficients for many key species remain unknown. In this paper, we consider (de)excitation of the hydroxyl and sulphanyl ions: OH^+ and SH^+, respectively. Both the species have electronic ground states of $^3\Sigma^-$ symmetry which adds an extra complication as the rotational levels display fine structure due to the electron spin of the two unpaired electrons and a hyperfine structure due to the nuclear spin of the hydrogen atom.

Both OH^+ and SH^+ were only detected in the interstellar medium (ISM) within the last decade; OH^+ being first observed by Wyrowski et al. (2010) and SH^+ by Benz et al. (2010) and Menten et al. (2011). However, the ions are now known to be widespread (Gerin, Neufeld & Goicoechea 2016). In particular, OH^+ has now been found in a variety of locations including translucent interstellar clouds (Gupta et al. 2010; Krełowski, Beletsky & Galazutdinov 2010) and both OH^+ and SH^+ have been recently observed in absorption across the $z = 0.89$ molecular absorber towards PKS 1830-211 (Muller et al. 2016, 2017). They have been also detected in emission in dense photon-dominated regions (PDRs) where electron collision processes are thought to be important (Nagy et al. 2013; van der Tak et al. 2013). A number of these observations resolve the fine (and sometimes hyperfine) structure in the transitions (Benz et al. 2010; Gerin et al. 2010; Godard et al. 2012; Nagy et al. 2013).

To date, the only one laboratory measurement of electron-impact rotational rate coefficients for a molecular ion was by Shafir et al. (2009) for HD^+; this experiment actually measured de-excitation and only gave enough information to show agreement with the theoretical predictions. This means that thus far astronomically important electron-impact rotational rate coefficients for molecular ions have all been computed (Faure & Tennyson 2001, 2003). In a recent paper (Hamilton et al. 2016), we used improved theory to compute rotational rate coefficients for three closed-shell hydride cations, ArH^+, CH^+, and HeH^+; these hydrides were chosen due to their significant role in the ISM, see Faure et al. (2017) for example. In this work, electron-impact rate coefficients are calculated for the open-shell ions OH^+ and SH^+. **R**-matrix calculations are combined with the adiabatic-nuclei-rotation (ANR) approximation to produce rotational cross-sections at electron energies below 5 eV. We also present electron-impact electronic excitation cross-sections for the two ions considered. While these are unlikely to be important for models of ISM, OH^+ can be found in planetary ionospheres (Fox et al. 2015), and cometary coma (Nordholt et al. 2003; Haider & Bhardwaj 2005; Rubin et al. 2009), as well as around Enceladus (Gupta et al. 2010). In these environments, electron-impact electronic excitation may well be important.

Section 2 describes the **R**-matrix calculations and the procedure used to derive the cross-sections and rate coefficients is briefly introduced. In Section 3, we present and discuss the calculated rate coefficients. A model for the excitation of OH^+ in the Orion bar PDR is also presented in Section 4. Conclusions are summarized in Section 5.

★E-mail: alexandre.faure@univ-grenoble-alpes.fr (AF); j.tennyson@ucl.ac.uk (JT)

Table 1. Vertical excitation energies for the lowest five excited states of OH^+ compared with measured adiabatic excitation energies.

State	This work (eV)	Previous (eV)
$X\,^3\Sigma^-$	0.000	0.000
$a\,^1\Delta$	2.509	2.190 [a]
$b\,^1\Sigma^+$	3.709	3.602 [b]
$A\,^3\Pi$	3.903	3.526 [b]
$1\,^1\Pi$	6.183	
$2\,^1\Sigma^+$	11.510	

[a]Katsumata & Lloyd (1977).
[b]Huber & Herzberg (1979).

2 R-MATRIX CALCULATIONS

Inelastic electron collision calculations with molecular ions OH^+ and SH^+ were performed using the R-matrix method (Tennyson 2010) within the Quantemol-N (Tennyson et al. 2007) expert system to run the UK molecular **R**-matrix codes (`UKRMol`) (Carr et al. 2012). Details follow closely the calculations performed in our previous paper (Hamilton et al. 2016), denoted I below, and are not repeated here. The calculations produce **T**-matrices which are processed by electron-impact rotational excitation code `ROTIONS` (Rabadán & Tennyson 1998), which employs the Coulomb-Born approximation to include the effects of high partial waves (Norcross & Padial 1982). In particular, $\Delta N = 1$ transitions (N is the molecular ion rotational angular momentum) are strongly influenced by the long-range dipole moment and `ROTIONS` uses the Coulomb-Born approximation to include the contributions of partial waves with $\ell > 4$. These long-range effects are unimportant for transitions with $\Delta N > 1$ (Faure & Tennyson 2001). Experimental values of the dipole moments were used in these calculations where available.

2.1 OH^+

The OH^+ target was represented using an augmented aug-cc-pVTZ GTO basis set. The use of augmented basis sets improves the treatment of the more diffuse orbitals for the excited states in the calculation. The ground state of OH^+ is $X\,^3\Sigma^-$ which has the configuration $[1\sigma\ 2\sigma\ 3\sigma]^6\ [1\,\pi]^2$. The target was represented using CAS-CI treatment freezing the lowest energy $1\sigma^2$ orbital and placing the highest six electrons in orbitals $[2\text{–}8\sigma, 1\text{–}3\,\pi]^6$. This target was constructed in an **R**-matrix sphere of radius 13 a_0. Nine electronically excited states were used in the close-coupling expansion.

The vertical excitation energies (VEEs) of the excited states of OH^+ calculated using this model at an equilibrium bondlength of 1.0289 Å are given in Table 1, where the VEEs are compared to measured values. The VEEs calculated in this work compare well to the measured adiabatic excitation energies (AEEs). VEEs naturally exceed AEEs and in this particular case the $A\,^3\Pi$ has a much larger equilibrium bondlength (1.134 Å) than the $b\,^1\Sigma^+$ state (1.032 Å), which results in a different order of the states at $R = 1.029$ Å. The excited states $a\,^1\Delta$, $b\,^1\Sigma^+$, and $A\,^3\Pi$ are within the electron energy range of interest in this investigation. Calculated equilibrium geometry dipole moment and rotational constant of OH^+ are compared to the best available values in Table 2.

Isotopic substitution shifts the centre-of-mass and hence, for ionic system, alters the permanent dipole moment. Oxygen exists in three isotopes giving $^{16}OH^+$, $^{17}OH^+$, and $^{18}OH^+$. While ^{16}O is the most abundant isotope, the abundance of ^{18}O is not negligible with an isotopic ratio $^{16}O/^{18}O$=498.7±0.1 for the Solar system (Vienna Standard Mean Ocean Water value) (Asplund et al. 2009; Meija et al. 2016). The abundance of ^{17}O is much lower with an isotopic ratio $^{16}O/^{17}O$=2632±7 (Asplund et al. 2009; Meija et al. 2016). To our knowledge, only the main isotopologue $^{16}OH^+$ has been detected in the ISM so far. For this reason, the discussion and results presented in the main paper will be concerned with only $^{16}OH^+$ (henceforth referred to as OH^+) but data for the other isotopologues are also included in the supplementary data to this article.

Table 2. Dipole moment, μ, and rotational constant, B, calculated for isotopologues of OH^+ are compared with published values.

Property	This work			Previous
	$^{16}OH^+$	$^{17}OH^+$	$^{18}OH^+$	$^{16}OH^+$
μ (D)	2.252	2.269	2.283	2.256 [a]
B (cm^{-1})	16.796	16.737	16.685	16.423 [b], 16.422 [c]

[a]Theory Werner, Rosmus & Reinsch (1983).
[b]Rotational spectroscopy Bekooy et al. (1985).
[c]Ultraviolet spectroscopy Merer et al. (1975).

Table 3. Vertical excitation energies for the lowest seven excited states of SH^+ compared with measured values.

State	This work (eV)	Previous (eV)
$X\,^3\Sigma^-$	0.000	
$a\,^1\Delta$	1.472	1.280 [a†], 1.340 [b†]
$b\,^1\Sigma^+$	2.517	2.390 [a†], 2.390 [b†]
$A\,^3\Pi$	3.856	3.740 [a†], 3.762 [c‡], 3.980 [b†]
		3.840 [b‡], 3.709 [d‡]
$c\,^1\Pi$	5.200	5.320 [a†], 4.722 [c‡], 5.220 [b†]
		4.800 [b‡]
$^5\Sigma^-$	9.817	9.090 [a†]
$2\,^3\Pi$	10.304	
$2\,^1\Sigma^+$	10.373	10.489 [b†]

† Adiabatic value.
‡ Vertical value.
[a]Observed, Dunlavey et al. (1979).
[b]Calculated, Bruna et al. (1983).
[c]Observed, Rostas et al. (1984).
[d]Observed, Horani, Leach & Rostas (1967).

2.2 SH^+

The SH^+ target was represented using a non-augmented Dunning cc-pVTZ GTO basis set. Unlike OH^+, an augmented basis set could not be used as it gave linear dependence problems and did not produce smooth results. The ground state of SH^+ has the configuration $[1\sigma\ 2\sigma\ 3\sigma\ 1\pi\ 4\sigma\ 5\sigma]^{14}\ [2\pi]^2$. The target was represented using CAS-CI treatment freezing electrons of the lowest energy 1–3σ and 1π orbitals and placing the highest six electrons in orbitals $[4\text{–}8\sigma, 2\text{–}4\,\pi, 1\,\delta]^6$. This target was constructed in an **R**-matrix sphere of radius 10 a_0. The VEEs of the excited states of SH^+ calculated from this model at the equilibrium bondlength of 1.3744 Å are given in Table 3 and compared to published values. The VEEs calculated in this work compare well to the measured VEEs. The calculated equilibrium geometry dipole moment and rotational constant of SH^+ are compared to the best available values in Table 4.

Sulphur exists as four isotopes giving $^{32}SH^+$, $^{33}SH^+$, $^{34}SH^+$, and $^{36}SH^+$. While ^{32}S is the most abundant isotope, the abundance of ^{34}S is significant with an isotopic ratio $^{32}S/^{34}S$∼22 for the Solar system (Asplund et al. 2009; Meija et al. 2016). The abundances of

Table 4. Dipole moment and rotational constant calculated for SH^+ compared with published values.

Property	This work				Previous
	$^{32}SH^+$	$^{33}SH^+$	$^{34}SH^+$	$^{36}SH^+$	$^{32}SH^+$
μ (D)	1.388	1.394	1.394	1.394	1.285 [a]
B (cm^{-1})	9.135	9.125	9.118	9.103	9.133 [b]

[a]Theory, Senekowitsch et al. (1985).
[b]Empirical, Müller et al. (2014).

the other isotopes are much lower with isotopic ratios $^{32}S/^{33}S \sim 125$ and $^{32}S/^{36}S \gtrsim 5000$ (Asplund et al. 2009; Meija et al. 2016). Both isotopologues $^{32}SH^+$ and $^{34}SH^+$ have been detected in the (extragalactic for $^{34}SH^+$) ISM (Muller et al. 2017). The discussion and results presented in the main paper will be concerned with only $^{32}SH^+$ (henceforth referred to as SH^+) but data for the other isotopologues are also included in the supplementary data to this article.

2.3 Cross-sections and rate coefficients

Working in C_{2v} symmetry, each of the above calculations produces eight fixed-nuclei **T**-matrices for each molecule: the four symmetries A_1, A_2, B_1, B_2 for both doublet and quartet states of the $N+1$ electron systems. These **T**-matrices are used to calculate the electronic excitation cross-sections using standard equations (Tennyson 2010) and, once converted to the $C_{\infty v}$ point group, rotational excitation cross-sections using the program ROTIONS (Rabadán & Tennyson 1998) using the rotational constants and isotope specific dipole moments given in Tables 2 and 4. ROTIONS computes the rotational excitation cross-sections for each doublet and quartet state independently. The total rotational cross-sections are thus obtained as the (weighted) sum of the doublet and quartet cross-sections.

2.3.1 *Electronic transitions*

Electronic excitation cross-sections were computed for collision energies $E_{\rm coll}$ in the range 0.01–5 eV. We consider electronic transitions from the ground state of each cation to all states with electronic thresholds below the 5 eV upper limit. The electronic thresholds are calculated using the fixed-nuclei approximation. Assuming that the electron velocity distribution is Maxwellian, rate coefficients for excitation transitions were obtained for temperatures in the range 1–5000 K.

2.3.2 *Rotational transitions*

As in I, we use a combination of the adiabatic nuclei rotation (ANR) method (Chang & Temkin 1970) with Coulomb-Born completion (for dipolar transitions only). To allow for threshold effect, we used an empirical correction: below the excitation threshold, cross-sections are set to zero, see Faure et al. (2006) for details. The validity of this approach was confirmed recently for HeH^+ where the full-rovibrational multichannel quantum defect theory calculations by Čurík & Greene (2017) were found in good agreement with the ANR/Coulomb-Born calculations of I.

Rotational transitions between levels with $N \leq 11$ were considered. However, transitions were restricted to $\Delta N \leq 8$ owing to the finite number of partial waves in the **T**-matrices ($\ell \leq 4$). Rotational excitation cross-sections were computed for collision energies $E_{\rm coll}$ in the range 0.01–5 eV. For transitions with a rotational threshold below 0.01 eV, cross-sections were extrapolated down to the threshold using a $1/E_{\rm coll}$ (Wigner's) law, as recommended by Faure et al. (2006). Rate coefficients for excitation transitions were obtained for temperatures in the range 1–3000 K assuming a thermal electron energy distribution. The principle of detailed balance was used to compute de-excitation rate coefficients.

2.3.3 *Hyperfine transitions*

As discussed in the introduction, the fine and hyperfine structures of the OH^+ and SH^+ ions are resolved in astronomical observations. It is therefore necessary to provide hyperfine-resolved rate coefficients for these two ions. In the Hund's case (b) coupling scheme, the fine structure levels are labelled by (N, j) where $\mathbf{j = N + S}$ is the total angular momentum quantum number and $S = 1$ is the electronic spin. The hyperfine structure levels are labelled by (N, j, F) where $\mathbf{F = j + I}$ is the hyperfine quantum number and $I = 1/2$ is the nuclear spin of the hydrogen atom. Each rotational level is thus split into three fine-structure levels ($j = N-1, j = N, j = N+1$) (except $N = 0$) and each fine-structure level is in turn split into two hyperfine levels ($F = j \pm 1/2$) (except $(N, j) = (1, 0)$). The fine and hyperfine splittings are ~ 1 and ~ 0.001 cm^{-1}, respectively, i.e. they are much lower than the rotational and collisional energies. Thus, assuming that the electronic and nuclear spins play a spectator role during electron–molecule collisions, hyperfine-resolved rate coefficients can be computed using the simple infinite-order-sudden (IOS) approximation. Within this approximation, which is similar in spirit to the ANR approximation, the pure rotational rate coefficients obey the following equation (Corey & McCourt 1983):

$$k^{\rm IOS}_{N\rightarrow N'}(T) = [N'] \sum_L \begin{pmatrix} N' & N & L \\ 0 & 0 & 0 \end{pmatrix}^2 k^{\rm IOS}_{0\rightarrow L}(T), \quad (1)$$

where $[N']$ represents $(2N'+1)$ and $(\ \ )$ is a Wigner '3-j' symbol. In practice, the rate coefficients $k_{N\rightarrow N'}(T)$ computed with ROTIONS do not strictly follow equation (1) due to the Coulomb-Born completion and the threshold correction applied to the cross-sections. Equation (1) is however satisfied to within 25 per cent, down to 10 K. Within the IOS approximation, the fine-structure rate coefficients can be obtained as follows (Corey & McCourt 1983; Lique, Bulut & Roncero 2016):

$$k^{\rm IOS}_{Nj\rightarrow N'j'}(T) = [NN'j'] \sum_L \begin{pmatrix} N' & N & L \\ 0 & 0 & 0 \end{pmatrix}^2 \begin{Bmatrix} N & N' & L \\ j' & j & S \end{Bmatrix}^2 \times k_{0\rightarrow L}(T), \quad (2)$$

where $\{\ \ \}$ is a '6-j' Wigner symbol and $k_{0\rightarrow L}(T)$ are the rotational rate coefficients computed with ROTIONS. Similarly, the hyperfine-resolved rate coefficients can be obtained as (Daniel et al. 2005; Lique et al. 2016)

$$k^{\rm IOS}_{NjF\rightarrow N'j'F'}(T) = [NN'jj'F'] \sum_L \begin{pmatrix} N' & N & L \\ 0 & 0 & 0 \end{pmatrix}^2 \times \begin{Bmatrix} N & N' & L \\ j' & j & S \end{Bmatrix}^2 \begin{Bmatrix} j & j' & L \\ F' & F & I \end{Bmatrix}^2 \times k_{0\rightarrow L}(T). \quad (3)$$

In practice, however, the hyperfine rate coefficients for transitions with $N \neq N'$ were computed as (Neufeld & Green 1994; Faure & Lique 2012)

$$k^{INF}_{NjF\rightarrow N'j'F'}(T) = \frac{k^{\rm IOS}_{NjF\rightarrow N'j'F'}(T)}{k^{\rm IOS}_{N\rightarrow N'}(T)} k_{N\rightarrow N'}(T). \quad (4)$$

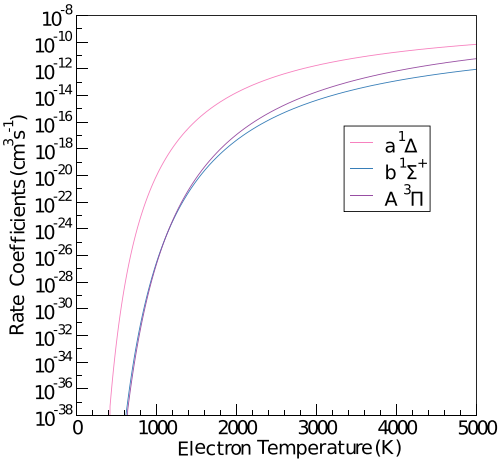

Figure 1. Rate coefficients for electronic excitation of OH^+.

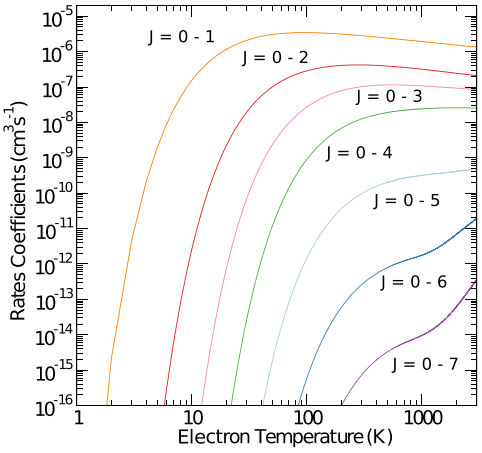

Figure 2. Rate coefficients for rotational excitation of OH^+ from the ground state (N=0) to the lowest seven excited states.

This scaling procedure guarantees the following equality:

$$\sum_{j'F'} k^{INF}_{NjF\to N'j'F'}(T) = k_{N\to N'}(T), \tag{5}$$

thus ensuring that the summed hyperfine rate coefficients are identical to the ANR/Coulomb-Born pure rotational rate coefficients. In addition, in order to improve the results at low temperatures, the fundamental excitation rate coefficients $k_{0\to L}(T)$ were replaced by the de-excitation fundamental rate coefficients using the detailed balance relation (within the IOS approximation) $k_{0\to L}(T) = [L]k_{L\to 0}(T)$, as in Faure & Lique (2012).

3 RESULTS

There are no previous studies on these systems against which we can compare. We start by considering results for electron-impact excitation of OH^+.

3.1 OH^+

Fig. 1 shows the rate coefficients for the electronic excitation of $OH^+(X\,^3\Sigma^-)$ after electron impact. This figure shows that the excitation of $OH^+(X\,^3\Sigma^-)$ to $OH^+(a\,^1\Delta)$ has a lower temperature threshold than the subsequent transitions and has a greater magnitude over the investigated temperature range. This is to be expected due to the electron energy threshold of this transition, as shown in Table 1. This figure also shows that while the rate coefficients for excitation to $OH^+(b\,^1\Sigma^+)$ and $OH^+(A\,^3\Pi)$ have a similar temperature threshold, the rate coefficient for excitation to $OH^+(A\,^3\Pi)$ dominates at higher temperatures and in fact is converging towards the rate coefficient for excitation to $OH^+(a\,^1\Delta)$. This is a consequence of the fact that the $OH^+(X\,^3\Sigma^-)$ to $OH^+(A\,^3\Pi)$ transition is dipole allowed so this excitation tends to dominate at high impact energies. State-to-state Einstein coefficients for the $^3\Sigma^- - {}^3\Pi$ band can be found in Gómez-Carrasco et al. (2014).

Fig. 2 presents rate coefficients for electron-impact rotational excitation of OH^+ from its rotational ground state. The processes are dominated by the $\Delta N = 1$ transition due to the long-range effect of the dipole moment discussed above. As ΔN increases, the temperature threshold of the process increases and the magnitude of the rate coefficients decreases.

Table 5 presents rate coefficients for electron-impact hyperfine de-excitation of OH^+ from the initial levels $(N, J, F) = (1, 2, 5/2)$ and $(1, 2, 3/2)$. These two levels are the upper states of the observed transition of OH^+ at 972 GHz that will be discussed in the next section. It can be noticed that transitions with $\Delta F = \Delta j = \Delta N = \pm 1$ are collisionally favoured, as observed previously for other $^3\Sigma^-$ targets colliding with neutrals (see Lique et al. 2016, and references therein). We note that radiatively the selection rule $\Delta F = 0, \pm 1$ holds strictly and transitions with $\Delta F = \Delta j = \Delta N$ are the strongest ones. We also observe that de-excitation rate coefficients decrease significantly with temperature, typically by a factor of 10 between 10 and 1000 K.

Table 5. Hyperfine de-excitation rate coefficients in cm^{3}s^{-1} for OH^+ in initial levels $(N, J, F) = (1, 2, 5/2)$ and $(1, 2, 3/2)$. Powers of 10 are given in parentheses.

N	j	F	N'	j'	F'	10 K	100 K	1000 K
1	2	5/2	0	1	3/2	5.38(−6)	1.72(−6)	6.39(−7)
1	2	5/2	0	1	1/2	0.0	0.0	0.0
1	2	5/2	1	0	1/2	3.81(−7)	1.16(−7)	3.80(−8)
1	2	3/2	0	1	3/2	8.97(−7)	2.87(−7)	1.06(−7)
1	2	3/2	0	1	1/2	4.48(−6)	1.43(−6)	5.32(−7)
1	2	3/2	1	0	1/2	3.81(−7)	1.16(−7)	3.80(−8)
1	2	3/2	1	2	5/2	2.00(−7)	6.09(−8)	1.99(−8)

3.2 SH^+

Fig. 3 shows the rate coefficients for the electronic excitation of $SH^+(X\,^3\Sigma^-)$ after electron impact. This figure shows that the temperature thresholds of the three transitions considered in this work are fairly similar. The rate coefficient for the transition to $SH^+(a^1\Delta)$ dominates from relatively low temperatures whereas the rate coefficients for transitions to $SH^+(b\,^1\Sigma^+)$ and $SH^+(A\,^3\Pi)$ remain very similar up to around 2000 K. At higher temperatures, the rate coefficient for the transition to $SH^+(b\,^1\Sigma^+)$ exceeds that for the transition to $SH^+(A\,^3\Pi)$. This latter does however tend to converge towards the former as the temperature increases still further.

Fig. 4 presents rate coefficients for electron-impact rotational excitation of SH^+ from its rotational ground state. The processes are again dominated by the $\Delta N = 1$ transition, particularly at low temperatures. As ΔN increases, the temperature threshold of the process increases and the magnitude of the rate coefficient decreases

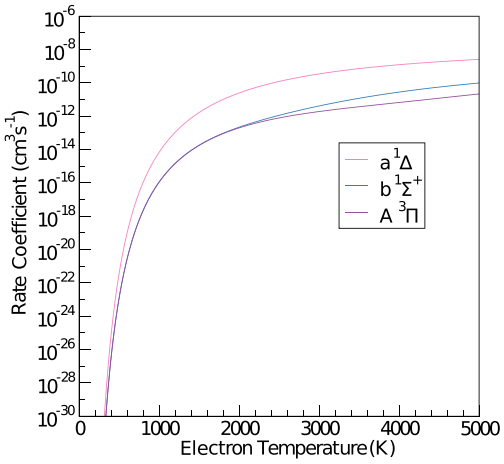

Figure 3. Rate coefficients for electronic excitation of SH^+.

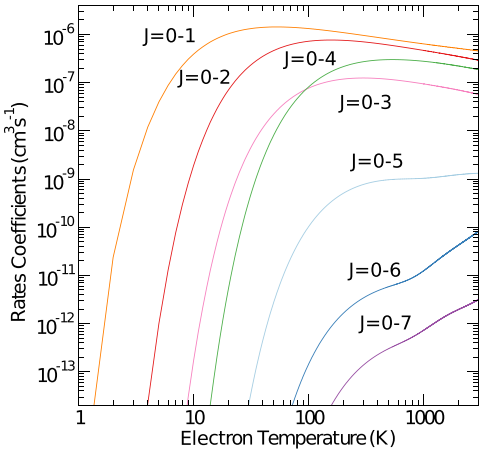

Figure 4. Rate coefficients for rotational excitation of SH^+ from the ground state (N=0) to the lowest seven excited states.

Table 6. Hyperfine de-excitation rate coefficients in cm^3s^{-1} for SH^+ in initial levels (N, J, F) = (1, 2, 5/2) and (1, 2, 3/2). Powers of 10 are given in parentheses.

N	j	F	N'	j'	F'	10 K	100 K	1000 K
1	2	5/2	0	1	3/2	1.80(−6)	5.75(−7)	2.18(−7)
1	2	5/2	0	1	1/2	0.0	0.0	0.0
1	2	5/2	1	0	1/2	4.04(−7)	1.27(−7)	4.04(−8)
1	2	3/2	0	1	3/2	3.00(−7)	9.58(−8)	3.63(−8)
1	2	3/2	0	1	1/2	1.50(−6)	4.79(−7)	1.82(−7)
1	2	3/2	1	0	1/2	4.04(−7)	1.27(−7)	4.04(−8)
1	2	3/2	1	2	5/2	2.12(−7)	6.68(−8)	2.12(−8)

with the exception of the rate coefficient for the $\Delta N = 4$ transition which comes to exceed that of the $\Delta N = 3$ transition above ∼90 K.

Table 6 presents rate coefficients for electron-impact hyperfine de-excitation of SH^+ from the initial levels (N, J, F) = (1, 2, 5/2) and (1, 2, 3/2). These two levels are the upper states of the transition of SH^+ at 526 GHz first detected with *Herschel* (Benz et al. 2010). Again, we can notice that transitions with $\Delta F = \Delta j = \Delta N = \pm 1$ are favoured and that de-excitation rate coefficients decrease by a factor of ∼10 between 10 and 1000 K.

The supplementary data associated with this paper include:

(i) Electronic excitation cross-sections and rate coefficients for $^{16}OH^+$ and $^{32}SH^+$. Data include all electronic states with thresholds below 5 eV.

(ii) Rotation excitation cross-sections and rate coefficients for the three isotopes of OH^+ and the four isotopes of SH^+. Rotational excitation data sets are published for transitions with starting values of $N = 0$ to $N = 11$.

(iii) Hyperfine de-excitation rate coefficients for $^{16}OH^+$, $^{18}OH^+$, and $^{32}SH^+$. Hyperfine de-excitation data sets are published for transitions with starting values of (N, j, F) = (0, 1, 3/2) to (11, 11, 21/2).

These data will also be placed in the BASECOL data base (Dubernet et al. 2013).

Hyperfine data for $^{16}OH^+$, $^{18}OH^+$, and $^{32}SH^+$ have been also combined with the spectroscopic data from the Cologne Database for Molecular Spectroscopy (CDMS) (Müller et al. 2005) in order to provide a full and consistent data set adapted to radiative transfer studies (see below). Hyperfine data for the other isotopologues are not provided due to the lack of spectroscopic data (the recent entry $^{34}SH^+$ at CDMS is currently limited to nine hyperfine transitions within N = 1–0).

4 OH^+ EXCITATION IN THE ORION BAR

The first detection of OH^+ in emission in a Galactic source was reported by van der Tak et al. (2013) using the *Herschel Space Observatory*. These authors presented line profiles and maps of OH^+ line emission towards the Orion Bar PDR. The Orion Bar PDR is the archetypal edge-on molecular cloud surface illuminated by far-ultraviolet radiation from nearby massive stars. The analysis of the chemistry and excitation of OH^+ by van der Tak et al. (2013) suggests an origin of the emission at visual extinctions $A_V \sim 0.1$–1 where most of the electrons are provided by the ionized carbon atoms and hydrogen is predominantly in atomic form. This is also the region where CH^+ and SH^+ emissions originate (Nagy et al. 2013). In such an environment, the dominant formation pathway for OH^+ is $O^+ + H_2$ and the main destruction route is $OH^+ + H_2$ (van der Tak et al. 2013). The reaction of OH^+ with H is endothermic. Chemical pumping may thus play a role in the excitation of OH^+ only if the molecular fraction $f(H_2) = 2N(H_2)/(2N(H_2) + N(H))$ is large enough. Given that $f(H_2)$ is expected to be low (< 10 per cent) in the PDR layers where OH^+ ions form, the impact of chemical pumping should be small, as found by Gómez-Carrasco et al. (2014). This is in contrast with CH^+ which reacts rapidly with H to form $C^+ + H_2$ (Faure et al. 2017).

We have thus assumed that the excitation of OH^+ is entirely driven by inelastic collisions with electrons and hydrogen atoms. The hyperfine collisional data presented above for $OH^+ + e^-$ and those of Lique et al. (2016) for $OH^+ + H$ were combined with spectroscopic data from CDMS and implemented in a non-LTE radiative transfer model. We have employed the public version of the RADEX code[1] which uses the escape probability formulation assuming an isothermal and homogeneous medium. The cosmic microwave background is the only background radiation field with a temperature of 2.73 K. Radiative pumping by local dust and starlight is neglected in order to focus on collisional excitation

[1] http://home.strw.leidenuniv.nl/~moldata/radex.html

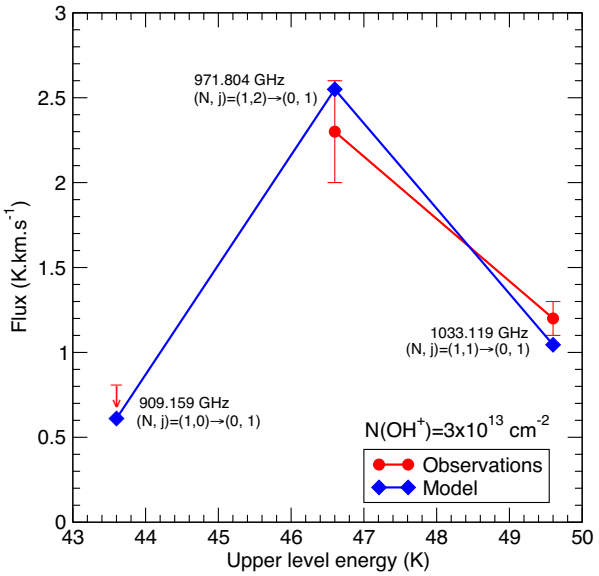

Figure 5. OH^+ line flux of the strongest hyperfine components of the transition $(N, j) = (1, j) \rightarrow (0, 1)$ as functions of the upper level energy, as predicted by our non-LTE calculations for the physical conditions used for the Orion Bar. The OH^+ column density was adjusted to best reproduce the observations of van der Tak et al. (2013). See the text for details.

effects. We assume that OH^+ probes a homogeneous region corresponding to the 'hot gas at average density' described by Nagy et al. (2017) for the Orion Bar: the atomic hydrogen density is taken as $n(\mathrm{H}) = 2 \times 10^5\,\mathrm{cm}^{-2}$ and the kinetic temperature as $T_\mathrm{k} = 500\,\mathrm{K}$, that is a thermal pressure of $10^8\,\mathrm{K\,cm}^{-3}$ which is typical of a dense PDR. We adopted a typical electron fraction $x(e) = n(e^-)/n(\mathrm{H}) = 10^{-4}$, as expected if carbon is fully ionized. The line width was fixed at $4\,\mathrm{km\,s}^{-1}$, as observed by van der Tak et al. (2013). Assuming a unit filling factor, the OH^+ column density is the single free parameter adjusted to best reproduce the integrated intensities measured by van der Tak et al. (2013). We have employed the three transitions observed by these authors at 909.159, 971.804, and 1033.119 GHz, corresponding to the transitions $(N, j, F) = (1, 0, 1/2) \rightarrow (0, 1, 3/2)$, $(1, 2, 5/2) \rightarrow (0, 1, 3/2)$, and $(1, 1, 3/2) \rightarrow (0, 1, 3/2)$, respectively, which are the strongest hyperfine components in each fine-structure line. It must be noted that the transition $(N, j, F) = (1, 2, 5/2) \rightarrow (0, 1, 3/2)$ is actually blended with the transition $(1, 2, 3/2) \rightarrow (0, 1, 1/2)$ at 971.805 GHz. Since RADEX does not treat the overlap of lines, it was necessary to extract the excitation temperature and line centre opacity of the blended transitions. Assuming Gaussian shapes, the opacities were summed to simulate a composite line whose intensity was integrated over a velocity range from -10 to $+10\,\mathrm{km\,s}^{-1}$. Overlap effects should be properly included in the radiative transfer treatment but given the low opacity of the lines ($\tau < 2$) their impact is expected to be moderate here.

Very good agreement is observed in Fig. 5 between our model and the observations for an OH^+ column density of $3 \times 10^{13}\,\mathrm{cm}^{-2}$. Indeed, the calculations agree, essentially within error bars, with *Herschel* data at 971.804 and 1033.119 GHz. They are also consistent with the upper limit at 909.159 GHz. Our column density is a factor of $\sim$3 lower than the value derived by van der Tak et al. (2013). These authors have employed similar physical conditions but different collisional data and they included chemical terms, which explains the difference. On the other hand, we note that our result is in good agreement with the column density derived by van der Tak et al. (2013) using the abundance predicted by the Meudon PDR code ($1.6 \times 10^{13}\,\mathrm{cm}^{-2}$). Finally, the contribution of electron collisions was found to be moderate, of the order of 10–20 per cent, at an electron fraction $x_\mathrm{e} = 10^{-4}$. The excitation of OH^+ in the Orion Bar is therefore dominated by hydrogen collisions. The impact of electron-impact excitation would be much larger in environments with high ionization fractions such as supernova remnants (Barlow et al. 2013; Hamilton et al. 2016) or planetary nebulae (Aleman et al. 2014).

5 CONCLUSIONS

Electronic and rotational excitation cross-sections and rate coefficients have been produced and made available for a range of rotational transitions of the open-shell hydrides OH^+ and SH^+ and their isotopologues. The electronic structure calculations were validated where possible against published data. The calculated excitation thresholds, calculated dipole transition moments, and rotational constants of both hydrides were validated against measured values or values recommended by the CDMS (Müller et al. 2005) and these comparisons are very good.

The **R**-matrix method was used to calculate **T**-matrices from which electronically and rotationally inelastic cross-sections were calculated. No published data were available to validate these inelastic cross-sections but the reliability of the ANR/Coulomb-Born approach was previously confirmed both experimentally and theoretically. Rate coefficients were calculated by integration of the cross-sections using Maxwell–Boltzman distribution of electron velocities. Hyperfine de-excitation rate coefficients were deduced from the rotational data using the IOS approximation. As with the closed-shell hydrides (Hamilton et al. 2016), the rotational excitation rate coefficients of the $\Delta N = 1$ transitions were found to be strongly influenced by the long-range effect of the dipole moment and have the largest magnitudes. This result was found to translate in the hyperfine propensity rule $\Delta F = \Delta j = \Delta N = \pm 1$.

The electron-impact excitation data were combined with the results of Lique et al. (2016) for OH^++H collisions in order to model the rotational/hyperfine excitation of OH^+ in the Orion Bar PDR. Very good agreement with the observations of van der Tak et al. (2013) was obtained for an OH^+ column density of $3 \times 10^{13}\,\mathrm{cm}^{-2}$, which is similar to the prediction of the Meudon PDR model. We recommend using the present data in any model of OH^+ excitation in regions where the electron fraction is larger than 10^{-4}.

Finally, electron collisions can seed processes besides rotational excitation and electronic excitation. For molecular ions, both dissociative recombination (DR) and vibrational excitation can be astrophysically important processes. The mechanisms for these differ somewhat from that considered above as their cross-sections are dominated by the contribution of resonances. They thus require rather more extensive theoretical procedures, see for example Little et al. (2014). We note that electron-impact vibrational excitation and DR rate coefficients for OH^+ have very recently been computed by Stroe & Fifirig (2018).

ACKNOWLEDGEMENTS

We thank Yohann Scribano for help at the start of this project and François Lique for helpful discussions. This work has been supported by an STFC CASE studentship, grant number ST/K004069, for JRH, the Agence Nationale de la Recherche (ANR-HYDRIDES), contract ANR-12-BS05-0011-01 and by the

CNRS national programme 'Physico-Chimie du Milieu Interstellaire'.

REFERENCES

Aleman I. et al., 2014, A&A, 566, A79
Asplund M., Grevesse N., Sauval A. J., Scott P., 2009, ARA&A, 47, 481
Barlow M. J. et al., 2013, Science, 342, 1343
Bekooy J. P., Verhoeve P., Meerts W. L., Dymanus A., 1985, J. Chem. Phys., 82, 3868
Benz A. O. et al., 2010, A&A, 521, L35
Bruna P. J., Hirsch G., Bunker R. J., Peyerimhoff S. D., 1983, in Berkowitz J., Groeneweld K. O., eds, Molecular Ions, Geometric and Electronic Structures. NATO ASI Series, Plenum, New York
Carr J. M. et al., 2012, Eur. Phys. J. D, 66, 58
Chang E. S., Temkin A., 1970, J. Phys. Soc. Japan, 29, 172
Corey G. C., McCourt F. R., 1983, J. Phys. Chem., 87, 2723
Čurík R., Greene C. H., 2017, J. Chem. Phys., 147, 054307
Daniel F., Dubernet M.-L., Meuwly M., Cernicharo J., Pagani L., 2005, MNRAS, 363, 1083
Dubernet M.-L. et al., 2013, A&A, 553, A50
Dunlavey S. J., Dyke J. M., Fayad N. K., Jonathan N., Morris A., 1979, Mol. Phys., 38, 729
Faure A., Lique F., 2012, MNRAS, 425, 740
Faure A., Tennyson J., 2001, MNRAS, 325, 443
Faure A., Tennyson J., 2003, MNRAS, 340, 468
Faure A., Kokoouline V., Greene C. H., Tennyson J., 2006, J. Phys. B: At. Mol. Opt. Phys., 39, 4261
Faure A. et al., 2017, MNRAS, 469, 612
Fox J. L., Benna M., Mahaffy P. R., Jakosky B. M., 2015, Geophys. Res. Lett., 42, 8977
Gerin M. et al., 2010, A&A, 518, L110
Gerin M., Neufeld D. A., Goicoechea J. R., 2016, ARA&A, 54, 181
Godard B. et al., 2012, A&A, 540, A87
Gómez-Carrasco S. et al., 2014, ApJ, 794, 33
Gupta H. et al., 2010, A&A, 521, L47
Haider S. A., Bhardwaj A., 2005, Icarus, 177, 196
Hamilton J. R., Faure A., Tennyson J., 2016, MNRAS, 455, 3281
Harrison S., Faure A., Tennyson J., 2013, MNRAS, 435, 3541
Horani I. M., Leach S., Rostas J., 1967, J. Mol. Spectrosc., 23, 115
Huber K. P., Herzberg G., 1979, Molecular Spectra and Molecular Structure. IV. Constants of Diatomic Molecules, Vol. 716. Van Nostrand Reinhold Company, New York
Jimenez-Serra I., Martin-Pintado J., Viti S., Martin S., Rodriguez-Franco A., Faure A., Tennyson J., 2006, ApJ, 650, L135
Katsumata S., Lloyd D. R., 1977, Chem. Phys. Lett., 45, 519
Krełowski J., Beletsky Y., Galazutdinov G. A., 2010, ApJ, 719, L20
Lique F., Bulut N., Roncero O., 2016, MNRAS, 461, 4477
Little D. A., Chakrabarti K., Schneider I. F., Tennyson J., 2014, Phys. Rev. A, 90, 052705
Meija J. et al., 2016, Pure Appl. Chem., 88, 265
Menten K. M., Wyrowski F., Belloche A., Güsten R., Dedes L., Müller H. S. P., 2011, A&A, 525, A77
Merer A. J., Malm D. N., Martin R. W., Horani M., Rostas J., 1975, Can. J. Phys., 53, 251
Müller H. S. P., Schlöder F., Stutzki J., Winnewisser G., 2005, J. Mol. Struct. (THEOCHEM), 742, 215
Müller H. S. P. et al., 2014, A&A, 569, L5
Muller S. et al., 2016, A&A, 595, A128
Muller S. et al., 2017, A&A, 606, A109
Nagy Z. et al., 2013, A&A, 550, A96
Nagy Z. et al., 2017, A&A, 599, A22
Neufeld D. A., Green S., 1994, ApJ, 432, 158
Norcross D. W., Padial N. T., 1982, Phys. Rev. A, 25, 226
Nordholt J. E. et al., 2003, Geophys. Res. Lett., 30, 1465
Rabadán I., Tennyson J., 1998, Comput. Phys. Commun., 114, 129
Rostas J., Horani M., Brion J., Daumont D., Malicet J., 1984, Mol. Phys., 52, 1431
Rubin M., Hansen K. C., Gombosi T. I., Combi M. R., Altwegg K., Balsiger H., 2009, Icarus, 199, 505
Senekowitsch J., Werner H. J., Rosmus P., Reinsch E. A., O'Neil S. V., 1985, J. Chem. Phys., 83, 4661
Shafir D. et al., 2009, Phys. Rev. Lett., 102, 223202
Stroe M. C., Fifirig M., 2018, J. Phys. B: At. Mol. Opt. Phys., 51, 025202
Tennyson J., 2010, Phys. Rep., 491, 29
Tennyson J., Brown D. B., Munro J. J., Rozum I., Varambhia H. N., Vinci N., 2007, J. Phys. Conf. Ser., 86, 012001
van der Tak F. F. S., Nagy Z., Ossenkopf V., Makai Z., Black J. H., Faure A., Gerin M., Bergin E. A., 2013, A&A, 560, A95
Werner H. J., Rosmus P., Reinsch E. A., 1983, J. Chem. Phys., 79, 905
Wyrowski F., Menten K. M., Güsten R., Belloche A., 2010, A&A, 518, A26

SUPPORTING INFORMATION

Supplementary data are available at *MNRAS* online.

supdat.tar.gz

Please note: Oxford University Press is not responsible for the content or functionality of any supporting materials supplied by the authors. Any queries (other than missing material) should be directed to the corresponding author for the article.

This paper has been typeset from a TEX/LATEX file prepared by the author.